

# Probing Dark Energy Anisotropy

Stephen A. Appleby<sup>1</sup> & Eric V. Linder<sup>1,2</sup>

<sup>1</sup> *Institute for the Early Universe WCU, Ewha Womans University, Seoul, Korea and*

<sup>2</sup> *Berkeley Lab & University of California, Berkeley, CA 94720, USA*

(Dated: October 29, 2018)

Wide area cosmological surveys enable investigation of whether dark energy properties are the same in different directions on the sky. Cosmic microwave background observations strongly restrict any dynamical effects from anisotropy, in an integrated sense. For more local constraints we compute limits from simulated distance measurements for various distributions of survey fields in a Bianchi I anisotropic universe. We then consider the effects of fitting for line of sight properties where isotropic dynamics is assumed (testing the accuracy through simulations) and compare sensitivities of observational probes for anisotropies, from astrophysical systematics as well as dark energy. We also point out some interesting features of anisotropic expansion in Bianchi I cosmology.

## I. INTRODUCTION

The time variation of the cosmic expansion gives key clues to the energy components of the universe, with the acceleration pointing to an unknown dark energy. As cosmological surveys cover more of the sky in more detail we can also examine spatial variation of the expansion and dark energy properties. Here we investigate anisotropy rather than inhomogeneities. While the cosmic microwave background radiation places tight constraints on any anisotropy, ensuring a close to isotropic global expansion, smaller scale pressure anisotropies that do not disrupt the global isotropy remain possible. In particular these can also arise from astrophysical systematics, but we can phrase this in terms of variations in the effective dark energy pressure, and explore detectable signatures.

In testing for anisotropy or consistency with isotropy we can ask which cosmological probes are most sensitive in what redshift ranges to such a hypothetical anisotropy, i.e. what constraints could be put on angular variations in the local dark energy equation of state. The dark energy equation of state, which can also be interpreted in terms of an anisotropic pressure, is of interest because of its close connection with fundamental properties of the physics behind dark energy. As we will see, it also gives close connections with exact solutions of anisotropic spacetimes such as Bianchi models.

Other work has explored dark energy anisotropy in terms of the small scale spatial inhomogeneities in its density [1], large scale anisotropies giving an overall ellipticity to the universe [2], and within specific models such as vector dark energy [3–10], elastic dark energy [11–13], noncommutativity [14], etc. Our approach uses exact solutions, similar to [15], as well as phenomenological line of sight anisotropy but global isotropy, similar to [16, 17], testing the difference, exploring further probes, considering sources of astrophysical systematics, and motivating the phenomenology with comparisons to exact Bianchi solutions. For early and other work on anisotropic spacetimes see [18–24].

In Section II we draw lessons from the exact solutions of Bianchi I cosmology to underscore the difficulty of

global anisotropy and to motivate a possible alternate approach to anisotropic dark energy. We apply the Raychaudhuri beam equation of light propagation in Sec. III and simulate how surveys using, e.g., supernova distances in different sky patches could constrain anisotropy. A line of sight anisotropic model reminiscent of the Dyer-Roeder [25] treatment of inhomogeneities is then investigated in Sec. IV to determine the sensitivity of a variety of cosmological probes to detecting anisotropic dark energy or astrophysical systematics. We conclude in Sec. V.

## II. EXACT SOLUTION: BIANCHI I COSMOLOGY

To assess the influence of both the global expansion and the line of sight conditions on light propagation we examine an anisotropic exact solution of the Einstein field equations. The Bianchi I cosmology has different expansion rates along the three orthogonal spatial directions, given by the metric

$$ds^2 = -dt^2 + a(t)^2 dx_a^2 + b(t)^2 dx_b^2 + c(t)^2 dx_c^2. \quad (1)$$

The model is homogeneous but anisotropic. This can arise from a homogeneous and isotropic density but anisotropic pressure, for example. We can choose the matter and radiation components to be isotropic but the dark energy pressure to be different along the three axes, with equation of state ratios  $w_i = P_i/\rho_{de}$ .

We begin by examining the global dynamics. Although the full sky angular average of the dark energy equation of state is  $\bar{w} = (w_a + w_b + w_c)/3$ , the average expansion rate  $\bar{H} = (H_a + H_b + H_c)/3$  does not behave exactly like in an isotropic universe with  $\bar{w}$ . To quantify this, define  $H_{\text{iso}}$  to be the isotropic, Friedmann-Robertson-Walker (FRW) expansion rate for a universe with the same present matter density (and dark energy density) and with isotropic dark energy equation of state  $\bar{w}$ . We can then rewrite the Einstein field equations in terms of the ratio  $h_i \equiv H_i/H_{\text{iso}}$  and explore the deviations from isotropy.

This gives rise to an autonomous system of equations

$$h'_a = \frac{3}{2}h_a - h_a^2 - \frac{1}{2}(h_a h_b + h_a h_c - h_b h_c) - \frac{3}{2}\Omega_{de}(w_b + w_c - w_a) + \frac{3}{2}\bar{w}h_a\Omega_{de,iso} \quad (2)$$

$$h'_b = \frac{3}{2}h_b - h_b^2 - \frac{1}{2}(h_b h_c + h_b h_a - h_c h_a) - \frac{3}{2}\Omega_{de}(w_c + w_a - w_b) + \frac{3}{2}\bar{w}h_b\Omega_{de,iso} \quad (3)$$

$$h'_c = \frac{3}{2}h_c - h_c^2 - \frac{1}{2}(h_c h_a + h_c h_b - h_a h_b) - \frac{3}{2}\Omega_{de}(w_a + w_b - w_c) + \frac{3}{2}\bar{w}h_c\Omega_{de,iso} \quad (4)$$

$$\Omega'_{de} = -\Omega_{de}[(1+w_a)h_a + (1+w_b)h_b + (1+w_c)h_c - 3 - 3\bar{w}\Omega_{de,iso}] \quad (5)$$

$$\Omega'_m = -\Omega_m[h_a + h_b + h_c - 3 - 3\bar{w}\Omega_{de,iso}], \quad (6)$$

where prime denotes  $d/d \ln a_{\text{iso}}$ . The isotropic scale factor is used as a measure of time; note it is not equal to the monopole anisotropic scale factor  $\bar{a} = (abc)^{1/3}$ . The time dependent dimensionless dark energy and matter densities  $\Omega_{de}$  and  $\Omega_m$  are defined as  $\Omega_i \equiv 8\pi G\rho_i/(3H_{\text{iso}}^2)$ , and  $\Omega_{de,iso}$  denotes the dark energy density in the isotropic case, with equation of state  $\bar{w}$ . Numerically we evolve equations (2-6) and use the Friedmann-like equation

$$h_a h_b + h_a h_c + h_b h_c = 3(\Omega_m + \Omega_{de}) \quad (7)$$

as a consistency check at each timestep.

Numerical solutions to the field equations appear in Fig. 1. The early universe appears isotropic, with deviations in the expansion rate along symmetry axis  $i$  of order  $(\bar{w} - w_i)\Omega_{de}$ . So when  $\Omega_{de} \ll 1$  the universe is effectively isotropic. As the dark energy becomes more dynamically important, the anisotropy grows. However, note there is a late time fixed point (for  $\bar{w} > -1$ ) such that the expansion rates go to constant offsets from the isotropic behavior. This is quite interesting: the universe does not ‘‘pancake’’ in terms of expansion rate (although the ellipticity does diverge), but rather it retains some memory of the isotropic state and remains nearly isotropic in some average sense.

The fixed point solutions can be calculated analytically to various orders in the equation of state anisotropy. Take the dark energy equation of state along the three symmetry axes to be

$$(w_a, w_b, w_c) = (\bar{w} - e - f, \bar{w} + e, \bar{w} + f). \quad (8)$$

Assuming both  $e$  and  $f$  are small compared to  $1 + \bar{w}$ , i.e.  $\Delta w \equiv |w_i - \bar{w}| \ll 1 + \bar{w}$ , the asymptotic solutions as we approach the limit  $a_{\text{iso}} \rightarrow \infty$  for the expansion rates  $h_i = H_i/H_{\text{iso}}$  normalized to the isotropic rate  $H_{\text{iso}}(\bar{w})$

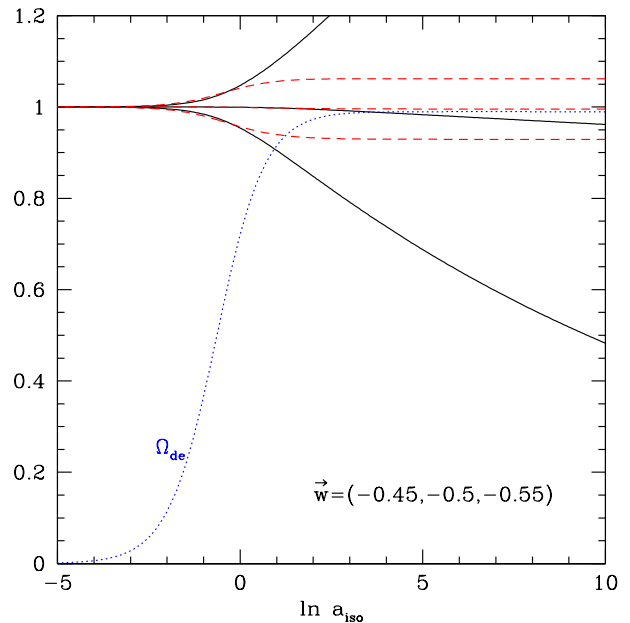


FIG. 1. Anisotropic expansion of a model with  $\vec{w} = (-0.45, -0.5, -0.55)$  is plotted vs  $\ln a_{\text{iso}}$  from the early to late universe. Solid black curves give the scale factors, and dashed red curves give the expansion rates, along the symmetry axes as ratios to an isotropic,  $\bar{w} = -0.5$  FRW universe. Early time and late time fixed points in expansion rate are seen.

are, to second order,

$$h_a = 1 - \frac{2(e+f)}{1-\bar{w}} - \frac{4}{3} \frac{e^2 + f^2 + ef}{1-\bar{w}^2} \quad (9)$$

$$h_b = 1 + \frac{2e}{1-\bar{w}} - \frac{4}{3} \frac{e^2 + f^2 + ef}{1-\bar{w}^2} \quad (10)$$

$$h_c = 1 + \frac{2f}{1-\bar{w}} - \frac{4}{3} \frac{e^2 + f^2 + ef}{1-\bar{w}^2} \quad (11)$$

$$\bar{h} = 1 - \frac{4}{3} \frac{e^2 + f^2 + ef}{1-\bar{w}^2} \quad (12)$$

$$\Omega_{de} = 1 - \frac{4}{3} \frac{(3-\bar{w})(e^2 + f^2 + ef)}{(1+\bar{w})(1-\bar{w}^2)}. \quad (13)$$

These expressions agree with the numerical results for the asymptotic expansion rates shown in Fig. 1 to 0.03%.

These solutions have several interesting properties. First, note that the averaged expansion rate  $\bar{h}$  deviates from the isotropic expansion rate only at second order in the equation of state anisotropy. Second, when the  $h_i$  approach fixed points, this means that  $H_i/H_{\text{iso}} = \text{constant}$ , not  $H_i = \text{constant}$ . When  $\bar{w} \approx -1$  and so  $H_{\text{iso}} \approx \text{constant}$  then as long as the offsets  $e, f$  are sufficiently small each  $H_i$  is nearly constant, i.e. one almost has de Sitter-like behavior.

This constancy of the expansion rate is reminiscent of the generic isotropization during inflation shown by [26]. There, anisotropic matter plus a cosmological constant led to eventual isotropic, de Sitter expansion while

here isotropic matter plus anisotropic dark energy leads to anisotropic expansion but one proportional to the isotropic case, and nearly de Sitter in the case that  $\bar{w} \rightarrow -1$ . Separately, note that  $\Omega_{de}$  goes asymptotically to a finite value different from 1, but the dimensionless matter density  $\Omega_m$  still goes to 0. The relation  $\Omega_{de} + \Omega_m = 1$  does not hold because these quantities were defined relative to  $H_{iso}$ , and  $\rho_{de}(w_a, w_b, w_c; t) \neq \rho_{de,iso}(\bar{w}; t)$ .

Cosmological models containing a global anisotropy, such as this Bianchi model, are severely constrained by observations [27–30], specifically the integrated Sachs-Wolfe effect on the CMB [31–33]. Illustratively, the temperature anisotropy arises as

$$\begin{aligned} \frac{\Delta T}{T} &\sim \int d\eta \delta g_{ij} \hat{n}^i \hat{n}^j \sim \int d\eta (a\dot{a} - b\dot{b}) \\ &\sim \int d\eta (h_a - h_b) \sim \int d\eta \Delta w, \end{aligned} \quad (14)$$

where  $\eta$  is the conformal distance,  $g_{ij}$  the metric, and  $\hat{n}$  the line of sight unit vector. More precisely, [3, 15] showed that for a dark energy model with constant equations of state ( $\bar{w} + \Delta w_a, \bar{w} + \Delta w_b, \bar{w} - \Delta w_a - \Delta w_b$ ),

$$\begin{aligned} \frac{\Delta T}{T} &= -J(\Omega_m, w) [\Delta w_a \sin^2 \theta \cos^2 \phi + \Delta w_b \sin^2 \theta \sin^2 \phi \\ &\quad - (\Delta w_a + \Delta w_b) \cos^2 \theta], \end{aligned} \quad (15)$$

where  $(\theta, \phi)$  parametrize the angular position on the sky and  $J(\Omega_m, w) \sim \mathcal{O}(1)$  is a function of the cosmological parameters. This equation highlights two important points: first that this anisotropic dark energy model sources the CMB quadrupole only (to leading order in  $\Delta w \ll 1$ ), and second that the temperature anisotropy is linearly proportional to  $\Delta w$  (as the cartoon version Eq. 14 also indicated). Therefore, barring any fine tuned cancellations of the leading order effect (such as through precisely compensated distributions of the energy-momentum, cf. the path integration over  $\Delta w$  in Eq. 14),  $|\Delta w| < 2 \times 10^{-4}$  is required for this Bianchi I class of models [15].

This conclusion seems difficult to avoid. However, let us investigate at what level other probes might independently constrain dark energy anisotropy within this model. Also note that the CMB constraint is an integrated effect from recombination to the present and so using only the late universe might also be of interest. To address those issues of possible compensation (such as might arise in vector field models [34]) or time-dependent low redshift anisotropy, in the next section we concentrate on supernova distances, observed over several well separated areas of sky, such as from the deep fields of Dark Energy Survey [35] or LSST [36].

### III. SUPERNOVA CONSTRAINTS ON ANISOTROPIC EXPANSION

Type Ia supernova (SN) distances provide excellent probes of the dark energy equation of state in isotropic

Friedmann-Robertson-Walker (FRW) universes. Here we apply them to an anisotropic universe such as the Bianchi I model just considered. (Also see [37] for fitting current data to a restricted Bianchi model.) The supernova survey is treated as independent sky areas with deep, well cadenced observations suitable for accurate distance measurement. We consider three patches of  $10 \text{ deg}^2$  each and study the effect of the angular distribution of the patches.

Within each area we simulate 1000 SN with magnitudes drawn from a Gaussian distribution with dispersion  $\sigma_m = 0.1$  and mean given by the isotropic expansion FRW relation with  $w = -1$ . The SN are randomly distributed between  $z = 0.2 - 1.2$ . This gives  $\sim 100$  SN per 0.1 redshift bin, or a statistical precision of 0.01 mag per bin. This is treated as the systematic floor, i.e. a survey may observe more SN in each patch but the effective error is equivalent to that of 1000 SN statistically.

Toward each patch we solve the light propagation in the anisotropic cosmology using the Raychaudhuri equation. First, the background expansion is given by the evolution equations

$$\begin{aligned} \dot{H}_a + H_a^2 + \frac{H_a H_b}{2} + \frac{H_a H_c}{2} - \frac{H_b H_c}{2} \\ = -4\pi G [P_b + P_c - P_a] \end{aligned} \quad (16)$$

$$\begin{aligned} \dot{H}_b + H_b^2 + \frac{H_b H_a}{2} + \frac{H_b H_c}{2} - \frac{H_a H_c}{2} \\ = -4\pi G [P_a + P_c - P_b] \end{aligned} \quad (17)$$

$$\begin{aligned} \dot{H}_c + H_c^2 + \frac{H_c H_a}{2} + \frac{H_c H_b}{2} - \frac{H_a H_b}{2} \\ = -4\pi G [P_a + P_b - P_c] \end{aligned} \quad (18)$$

$$\dot{\rho}_m + (H_a + H_b + H_c)\rho_m = 0 \quad (19)$$

$$\begin{aligned} \dot{\rho}_{de} + (1 + w_a)H_a\rho_{de} + (1 + w_b)H_b\rho_{de} \\ + (1 + w_c)H_c\rho_{de} = 0, \end{aligned} \quad (20)$$

which are basically Eqs. (2)–(6). These are solved starting with isotropic initial conditions  $a = b = c = a_i$  and  $H_a = H_b = H_c = H_{iso}$  at  $a_i = 2.5 \times 10^{-3}$  and evolved to the present, defined as  $\Omega_{de,0} = 0.72$ .

Once we have  $H_{a,b,c}$  and  $a, b, c$  this provides the redshift to each SN as a function of sky direction  $z(\theta, \phi)$ , and the Raychaudhuri equation can be used to determine the propagation of light rays through an arbitrary spacetime:

$$\frac{(A^{1/2})_{\lambda\lambda}}{A^{1/2}} + \frac{\zeta^2}{A^2} = -\frac{1}{2}R_{\mu\nu}k^\mu k^\nu \quad (21)$$

$$\zeta_\lambda = A\Theta \cos(\phi_\star - \phi) \quad (22)$$

$$\zeta\phi_\lambda = A\Theta \sin(\phi_\star - \phi), \quad (23)$$

where  $A^{1/2}$  is the cross sectional area of the beam,  $\zeta$  the amplitude of the shear, and  $\phi$  its phase. Subscripts  $\lambda$  denote derivatives with respect to the affine parameter  $\lambda$ , the photon four-momentum  $k_\mu$  is defined by  $k^\mu = dx^\mu/d\lambda$ ,  $R_{\mu\nu}$  is the Ricci tensor and

$$\Theta e^{i\phi_\star} = R_{\mu\alpha\nu\beta}k^\mu k^\nu (t^\star)^\alpha (t^\star)^\beta, \quad (24)$$

where  $R_{\mu\alpha\nu\beta}$  is the Riemann tensor and  $t^\mu$  is a complex null vector, defined via  $t^\mu t_\mu = t^\alpha k_\alpha = 0$  and  $t^\alpha (t^\star)^\alpha = 1$ . We use initial conditions  $A^{1/2} = 0, \zeta = 0$ .

The area of the light ray bundle  $A^{1/2}$  is linearly proportional to the angular diameter distance. For an isotropic spacetime Eq. (21) reduces to the standard result

$$d_A = \frac{\eta}{1+z} = \frac{1}{1+z} \int_0^z \frac{d\bar{z}}{H(\bar{z})}. \quad (25)$$

However, when we introduce anisotropy this relation is no longer correct due to the shear on the beam and the anisotropic part of the energy-momentum tensor (recall  $R_{\mu\nu}k^\mu k^\nu = T_{\mu\nu}k^\mu k^\nu$ ). The relation  $d_L = (1+z)^2 d_A$  does hold though regardless of the anisotropy, and we use this to construct the luminosity distance to each SN. For simplicity, we use the reasonable approximation that the globally anisotropic (Bianchi) expansion is effectively isotropic within each  $10 \text{ deg}^2$  patch of the sky (i.e. within this  $2.5 \times 10^{-4}$  of the full sky).

Note that the redshift now contains a non-trivial angular dependence

$$1+z(\theta, \phi, a, b, c) = \left( \left[ \frac{a(t_0)}{a} \right]^2 \sin^2 \theta \cos^2 \phi + \left[ \frac{b(t_0)}{b} \right]^2 \sin^2 \theta \sin^2 \phi + \left[ \frac{c(t_0)}{c} \right]^2 \cos^2 \theta \right)^{1/2}, \quad (26)$$

so we must obtain the luminosity distances as a function of redshift in each patch of the sky independently. In addition, we do not set  $a(t_0) = b(t_0) = c(t_0) = 1$  at the present, instead we choose isotropic initial conditions for the scale factors.

We perform an MCMC analysis to confront the anisotropic model with the simulated SN data. Figures 2–3 exhibit the constraints placed on the dark energy equation of state anisotropy. We have fixed  $\Omega_{de,0} = 0.72$  (and always assume spatial flatness), both to reflect the constraints coming from the much wider part of the surveys (i.e. the wide fields, rather than deep SN fields) and to find the maximum constraint on the anisotropy. Varying over more cosmological parameters would inevitably widen the uncertainty on  $(w_a, w_b, w_c)$  and hence obfuscate our point; to find the ceiling on how well a future supernova experiment could constrain the anisotropy.

In Fig. 2 we consider the patches to lie in the same quadrant of the sky, specifically  $(\theta, \phi) = (0, 0), (0.15, 0.15), (0.25, 0.25)$ , with the angles measured in radians. We do not expect such a setup to be optimal for constraining global anisotropy; if all of the patches constrain  $(\Delta w_a, \Delta w_b, \Delta w_c)$  in a similar direction then degeneracies should arise. However, surveys do sometimes select deep, cadenced fields within a restricted sky area.

The optimal constraint, using fields in orthogonal directions  $(\theta, \phi) = (0, 0), (0, \pi/2), (\pi/2, \pi/2)$  is shown in Fig. 3. We see that the constraints are much tighter and less degenerate. Generically we expect maximal degeneracy between the equation of state parameters when the patches align in the sky, and we require at least three patches to ensure that the degeneracy is broken.

We see that in the optimal case the constraints that upcoming SN surveys will be able to place on the global anisotropy are of order  $\Delta w \sim \mathcal{O}(10^{-2})$ . This is still significantly weaker than the ISW bound considered in [31–33]. Due to the prohibitive nature of the CMB limit for anisotropic expansion, barring fine tuning, in what follows we fix the global dynamics as isotropic and explore possible local, line of sight effects (including those due to systematics).

#### IV. LINE OF SIGHT APPROACH TO ANISOTROPY

Going from an anisotropic theoretical model to observational predictions is relatively straightforward, but we often want to proceed from (possibly anisotropic) observations to learn about the underlying cosmology. This entails some subtleties, which we begin by discussing before assessing the sensitivity of observational probes. Note that one of the points of interest is that tests of anisotropic measurements apply not only to non-FRW models but to isotropic universes with anisotropic astrophysical systematics (such as patchy extinction and others discussed below).

##### A. Testing Isotropy and Anisotropy

The previous sections discussed a simple anisotropic model of dark energy, and considered how a future survey might place constraints on the cosmological parameters characterizing the anisotropy (the three orthogonal equations of state). Since we had a definite cosmological model and a closed system of equations, we were able to directly relate expansion observables to the cosmological parameters.

Typically however, a different approach is taken when constraining anisotropy. The method in [16, 17] for example is to observe different patches of the sky, and assume an FRW-like evolution in each direction. Specifically, the luminosity distance in each direction  $\hat{n}$  is taken to be

$$d_L(\hat{n}) = \frac{1+z}{H_0} \int_0^z \frac{dz'}{\sqrt{\Omega_{m,0}(1+z')^3 + \Omega_{de,0}(1+z')^{3[1+w(\hat{n})]}}}. \quad (27)$$

Isotropy is tested by comparing the best fit parameter values  $w$  in each patch (usually other parameters such as  $\Omega_{m,0}$  are taken to be direction independent).

If the Universe (or more precisely, the data) is anisotropic, then it is important to realise that constraining the effective expansion history along a line of sight using a Friedmann equation is not a self consistent procedure. In the above example, if there were an anisotropic signal in the expansion data (the SN distances, say) then  $w$  along each line of sight in Eq. (27) does not correspond to the actual cosmological equation of state parameter that drives the expansion.

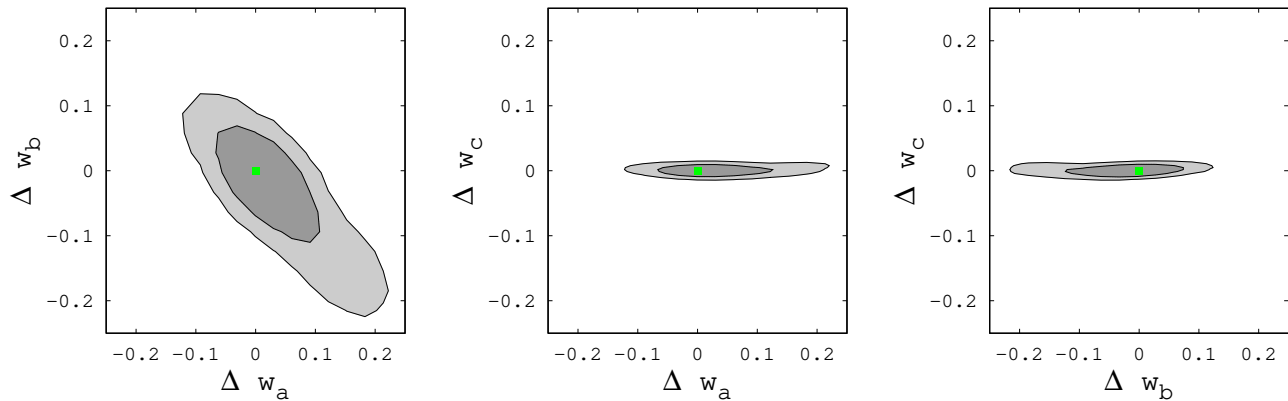


FIG. 2. 68% and 95% confidence level constraints on anisotropies ( $\Delta w_a, \Delta w_b, \Delta w_c$ ) obtained through MCMC analysis of distance measurements are shown for the case of three patches in the same quadrant of the sky. Such clustered fields yield large degeneracies. The isotropic input cosmology is denoted by the green square.

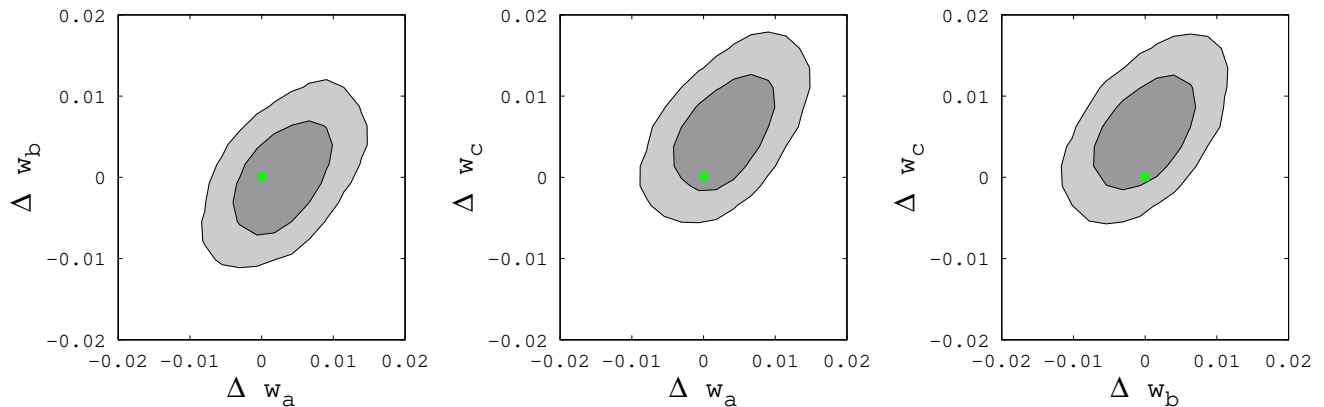


FIG. 3. As Fig. 2 but for the case of three patches in orthogonal sky directions. Note the change in scale. Now the equation of state estimations are strongly constrained and much less degenerate.

One can think of this approach as a “line of sight” method, similar in spirit to the Dyer-Roeder model [25] to test homogeneity. There, one takes a globally Friedmann expansion history but posits that along certain lines of sight the light bundles will feel a different matter distribution. In Eq. (27) one also assumes a globally Friedmann expansion, and yet allows  $w$  to vary with direction. This is an acceptable procedure as a consistency test of whether the isotropic FRW cosmology can fit the data. However to explore anisotropic models, and robustly deal with anisotropic signals in the data, one must find a way of relating the purely phenomenological  $w(\hat{n})$  in Eq. (27) to the physical expansion (i.e. the actual equation of state) in the proposed anisotropic model.

For the Bianchi I spacetime, the connection between the anisotropic distance-redshift relation and the dark energy equation of state is straightforward; it is provided by Eqs. (16-24). Note that even if we can relate  $w(\hat{n})$  to an actual cosmology, we still cannot generically use the standard relationship Eq. (27). This expression does not take

into account the redshift angular dependence  $z = z(\theta, \phi)$  of Eq. (26) or the beam shear that alters the angular diameter distance in the presence of an anisotropic fluid component. For astrophysical origins of anisotropy (see the next subsection for examples), adjustments must often be made quite early in the data analysis, e.g. extinction corrections enter in the lightcurve parameter fitting stage for SN rather than in the final distances.

Given the above issues, two questions should be addressed concerning the line of sight approach: 1) False positives – if the data is genuinely isotropic how accurately will the analysis be able to verify this and constrain anisotropies?, 2) False negatives – if the data is actually anisotropic, how accurately will the analysis be able to measure this, and rule out isotropy, given that the method is only consistent for isotropic data? Finally, if the method behaves well enough that we accept its formal shortcomings, then how sensitive are the various late time cosmological probes to anisotropies in the data.

The first question can be addressed by populating our

mock supernova sample using an isotropic cosmological model, and then performing an MCMC analysis using the full Bianchi machinery to fit  $(w_a, w_b, w_c)$  of the space-time, or using the line of sight approach to fit  $(w_1, w_2, w_3)$  of the patches, and testing each for isotropy. The relative magnitudes of the errors obtained using the two methods will inform us as to the reliability of the line of sight approach. The input cosmology is  $\Lambda$ CDM and we use similar SN data characteristics as in Sec. III. Both approaches reproduce the input cosmology, as expected, and the errors are of the same order of magnitude, although the line of sight approach gives  $\sim 50\%$  larger uncertainties on  $\Delta w$  ( $6 \times 10^{-3}$  rather than  $4 \times 10^{-3}$ , likely due to treating the parameters as independent in each field). We conclude that the line of sight approach is a viable method of testing isotropic data, despite the fact that it does not consistently take into account cosmological anisotropy.

The second question, that of false negatives, i.e. deriving isotropy spuriously because of using an (isotropic) FRW expression for distance, can be addressed by populating three patches in the sky using an anisotropic cosmological model, and then performing an MCMC analysis of the parameter space for the two different approaches. Specifically, we use the full Bianchi I equations to construct the magnitudes of 3000 supernovae in three orthogonal patches in the sky, using equation of state parameters  $(\Delta w_a, \Delta w_b, \Delta w_c) = (-0.04, 0, 0.04)$ , with respect to  $\bar{w} = -1$ . We then employ the full Bianchi I equations in the first approach, and the line of sight equations in the second. Figure 4 exhibits the results. The gray shaded confidence contours are obtained using the full anisotropic equations; as expected the best fit is very close to the input cosmology and we are able to distinguish this model from isotropic  $\Lambda$ CDM at high confidence.

The contours corresponding to the line of sight approach are presented as dashed lines; here we see a significant bias in the best fit value obtained in the analysis. This is due to the fact that the Hubble parameters  $H_{a,b,c}$  along each line of sight are not simply sourced by  $w_{a,b,c}$  individually and independently, but rather by linear combinations of them (see Eqs. (16 – 18)). Hence we are effectively constraining  $(w_b + w_c - w_a, w_a + w_c - w_b, w_a + w_b - w_c)$ , though we only realize that by using the Bianchi analysis not the Friedmann, and hence the best fit is biased. This is not the only difference between the methods however; the line of sight approach also does not take into account anisotropic effects such as beam shear or the non-trivial relationship between  $z$  and  $a, b, c, \theta, \phi$ . These differences account for the fact that the errors obtained using the two methods are different, and the line of sight approach yields perfectly non-degenerate contours.

In spite of the problems with the line of sight approach, it is clear that if there is anisotropy in the data then the method should detect it. That is, no triplet of the linear combinations of  $w_i$  will have all the same elements unless all individual  $w_i$  are identical, so false negatives

are avoided. How one interprets the anisotropy signal without knowing the underlying cosmological model is not clear however. In this work, we can roughly relate the line of sight method to cosmological parameters since we have created the data using a specific anisotropic model. With real data, we no longer have the luxury of knowing the source of the anisotropy.

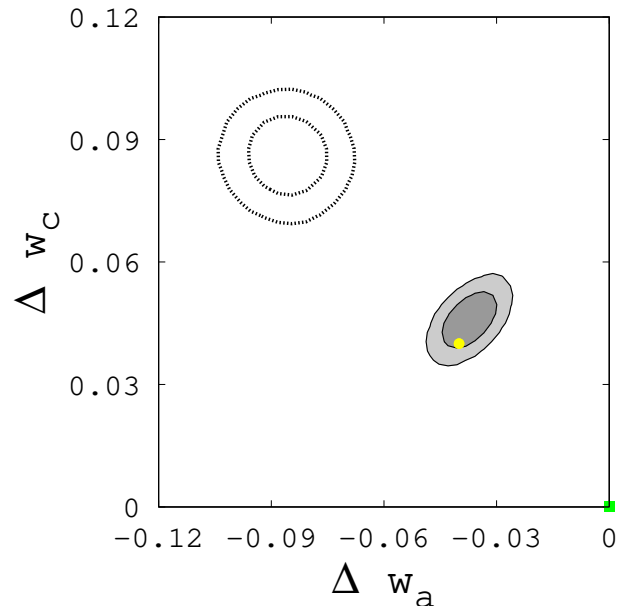


FIG. 4. 68% and 95% CL contours are presented for fitting for an anisotropic input cosmology when solving the full Raychaudhuri cosmological equations (gray shaded contours) and when using the line of sight approach (unfilled dotted contours). Both approaches accurately reject the isotropic,  $\bar{w} = -1$  case (green square) and the Raychaudhuri method recovers the input cosmology (yellow dot). The line of sight method actually constrains combinations of the  $w_i$  (but this is not realized without knowing the true cosmology). The other 2D projections not shown look similar.

There is one final effect that must be considered. In the above analysis we have taken the supernova deep fields to lie in orthogonal directions. This will provide a maximal constraint on the anisotropy of the data, however it is also expected to be the setup for which the two approaches will have closest agreement. This is due to the fact that in the line of sight approach, we are assuming that the directional dependent equation of state parameters are uncorrelated. However, if the fields are all located in the same region, then we expect an additional deviation between the two methods as a result of the correlation between the fields' equations of state, although such fields will also deliver poorer constraints.

## B. Sensitivity to Anisotropy

The line of sight approach is therefore adequate for testing isotropy and (the presence of) anisotropy. Moreover, it permits exploration not only of anisotropy from the cosmological model but from astrophysical systematics. For example, measurements of supernova distances in directions with different extinctions would imply different cosmological parameters for the distance-redshift relation if the patchy extinction was not fully recognized. Indeed, at the levels of accuracy required for future distance measurements, work is still ongoing in mapping inhomogeneous dust extinction in our Milky Way galaxy [38]. Another example is baryon acoustic oscillation (BAO) scale distances measured through galaxy clustering. Anisotropic stellar density can either obscure or augment the galaxy clustering correlation function if not fully recognized [39]; indeed before correction this gives a  $2.6\sigma$  difference between the BAO scale measured from Northern Galactic Cap and Southern Galactic Cap fields (see Appendix A of [40]). Other possible astrophysical anisotropies include a locally anisotropic electron optical depth in CMB measurements (e.g. see [41] and references therein) and patchy reionization, which can affect CMB, 21 cm, and even BAO cosmology inferences [42–46].

The question we consider now is how sensitive various late time cosmological probes are to any such anisotropy, and over which redshifts. We emphasize that  $\Delta w$  is merely a proxy, a common language, for comparing such sensitivities, and may have nothing to do with a physical equation of state. The probes considered are the distance-redshift relation  $d(z)$ , e.g. as measured through Type Ia supernovae or baryon acoustic oscillations, the Hubble parameter  $H$ , e.g. through radial BAO, and the reduced distance to CMB last scattering  $d_{lss}$ . We also consider probes of growth variables such as the growth factor  $g = D/a = (\delta\rho_m/\rho_m)/a$  normalized to one at high redshift, e.g. as measured from weak gravitational lensing or galaxy surveys, and the growth rate  $f = d\ln D/d\ln a$  in the products  $f\sigma_8(z) \sim fD$  and  $f\sigma_8/\sigma_{8,0}$ , calibrated to high redshift and low redshift, respectively, e.g. from redshift space distortions.

Figure 5 exhibits the sensitivities to anisotropies  $\Delta w$  between lines of sight as a function of the redshift  $z$  of the measurement, for 1% accuracy on different observable quantities  $\mathcal{O}$ . That is,

$$\Delta w_{1\%} = \left( \frac{\partial \mathcal{O}}{\partial w} \frac{1}{0.01\mathcal{O}} \right)^{-1}. \quad (28)$$

Again,  $\Delta w$  means that level of variation in the observable from any anisotropy source equivalent to a change  $\Delta w$ . Seeing anisotropies that have smaller  $\Delta w$  than in the Figure would require better than the 1% measurement accuracy. The assumption here is that this is a differential measurement on the sky, and the overall wide field survey determines the background values of all other cosmological parameters. Thus the figure gives lower lim-

its on the sensitivity to anisotropy  $\Delta w$  between different lines of sight.

One must fold into the figure the level of accuracy which a particular observable quantity would actually attain. For example, the CMB distance  $d_{lss}$  may be measured by the Planck satellite to 0.2% [47], while  $H$  is generally measured less well than  $d$  from BAO. Furthermore, the precisions must be scaled to reflect the area of sky used to compare lines of sight. The 0.2% precision for  $d_{lss}$  is for full sky, but to look for anisotropy one must split up the area into patches, so the precision would degrade.

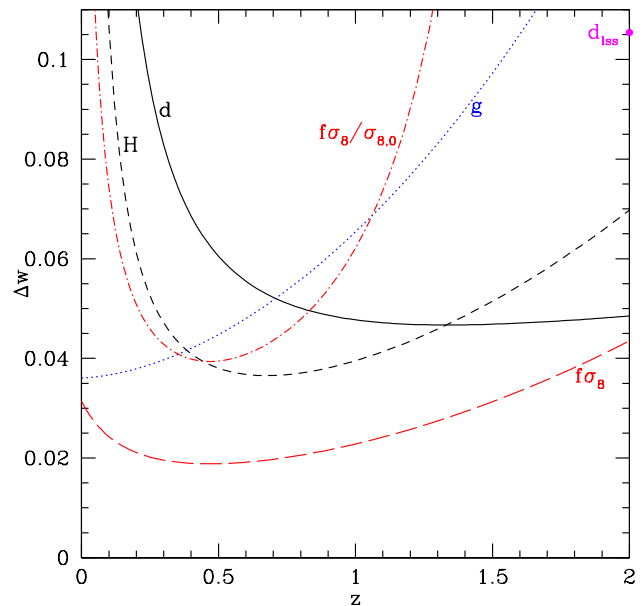


FIG. 5. Each curve represents the sensitivity  $\Delta w$  to dark energy anisotropy made possible by 1% measurements of the labeled observable, as function of measurement redshift. The CMB  $d_{lss}$  sensitivity is shown on the right axis by the purple filled circle.

For some probes the angular scales of sensitivity to anisotropy are limited by the nature of the observable. For example, both CMB acoustic peaks and BAO have angular sizes of  $\sim 1$  degree, so they lose sensitivity to anisotropies on smaller scales. On the other hand, supernovae or weak lensing, for example, can probe down to smaller scales. We expect higher derivative quantities such as growth rates relative to growth, or the Hubble parameter relative to distance, to be less accurately measured.

Taking these various factors into account, from Fig. 5 we anticipate that the most sensitive probe of such anisotropy will be supernova distance measurements, with possibly low redshift growth factor measurements from weak lensing and the growth rate from redshift space distortions contributing, especially to small scale anisotropy constraints. Large surveys, both spectro-

scopic and photometric, play roles in constraining dark energy anisotropy (including through determining the other background quantities). Photometric errors propagate through to roughly the same errors in distance, i.e.

$$\frac{\Delta d_l}{d_l} = \frac{\Delta z}{1+z} \left[ 1 + \frac{(1+z)^2}{Hd_l} \right] \approx \frac{\Delta z}{1+z}, \quad (29)$$

so as long as photometric errors in a redshift bin composed of many objects can be constrained well, the distance uncertainties will be controlled sufficiently to allow testing anisotropy. Thus, a wide field galaxy, or supernova, survey such as LSST could be used to investigate anisotropic properties of dark energy, as studied empirically in [16].

## V. CONCLUSIONS

The cosmic microwave background radiation delivers strong evidence for isotropy, restricting global anisotropy to the  $\sim 10^{-5}$  level. This severely disfavors anisotropic models such as a Bianchi I universe. Lower redshift wide field surveys can deliver constraints at the percent level. Preserving isotropic expansion dynamics but allowing for local anisotropy remains a possibility, at least on a phenomenological level. This Ansatz is similar to that of the Dyer-Roeder model, where global dynamics can stay Friedmann-Robertson-Walker despite lines of sight having differing properties.

We have calculated exact solutions of the anisotropic Bianchi I cosmology and shown that even in the case of extreme anisotropy the expansion can retain FRW-like characteristics. Indeed, the expansion rate in different directions does not have to diverge, but can go to fixed points. We give analytic expressions for these through second order in the dark energy equation of state anisotropy. The average expansion rate equals the expansion rate of the associated FRW universe at first order.

Carrying out Monte Carlo simulations of deep fields within a wide field survey, à la Dark Energy Survey or LSST, we study the effect of the configuration of deep field distance measurements on the global anisotropy constraints. Sky areas that are well separated in orthogonal directions break degeneracies and give tight constraints.

Adopting a phenomenological Ansatz with direction dependent pressure (or equation of state) but global isotropy requires careful thought. However, the results of our Bianchi I analysis help motivate that an Ansatz retaining a globally isotropic expansion could serve as

a reasonable approximation, and our Monte Carlo results show that the line of sight approach, handled carefully, can give consistent results for isotropy or an alarm for anisotropy (including astrophysical systematics). We stress that when using the line of sight approach, one cannot interpret an anisotropic signal in terms of cosmological parameters in a straightforward manner.

We then investigated the constraints that different astrophysical observations could place on such anisotropy. For small angular scales, supernova distances and redshift space distortions have good leverage, while on large angular scales BAO and CMB distances impose limits. Both spectroscopic and photometric surveys can contribute constraints, with next generation surveys capable of limiting anisotropies (described in the proxy language of dark energy equation of state  $\Delta w$ ) at the  $\sim 5\%$  level at each redshift (with tighter constraints from summing over a redshift range).

We emphasize several caveats. A definite model for anisotropic dark energy that preserves isotropic expansion to the level required by the CMB requires further work. Standard inhomogeneous perturbations, from a low sound speed for example, do not suffice. The pressure perturbations may be decoupled though from the density ones by adopting an infinite sound speed such as in the cuscuton model [48]. Large surveys give strong constraints but must be subdivided into patches to compare the equation of state along different lines of sight, diluting their effective volume. We have outlined a number of systematics that are direction dependent, such as patchy extinction or gravitational lensing, and could give spurious signals for line of sight variation. This article demonstrates some interesting features and results regarding testing dark energy anisotropy but also applies, probably more realistically, to astrophysical systematics.

## ACKNOWLEDGMENTS

We thank Richard Battye, David Rubin, David Schlegel, Tristan Smith, and Hu Zhan for useful discussions. This work has been supported by World Class University grant R32-2009-000-10130-0 through the National Research Foundation, Ministry of Education, Science and Technology of Korea, and in part by the Director, Office of Science, Office of High Energy Physics, of the U.S. Department of Energy under Contract No. DE-AC02-05CH11231.

---

[1] A. R. Cooray, D. E. Holz and R. Caldwell, JCAP **1011** (2010) 015 [[arXiv:0812.0376](#) [astro-ph]].  
 [2] T. Koivisto and D. F. Mota, Astrophys. J. **679**, 1 (2008) [[arXiv:0707.0279](#) [astro-ph]].

[3] T. Koivisto and D. F. Mota, JCAP **0806**, 018 (2008) [[arXiv:0801.3676](#) [astro-ph]].  
 [4] T. S. Pereira, C. Pitrou and J. P. Uzan, JCAP **0709**, 006 (2007) [[arXiv:0707.0736](#) [astro-ph]].



- [5] J. Beltran Jimenez and A. L. Maroto, Phys. Rev. D **78** (2008) 063005 [[arXiv:0801.1486](#) [astro-ph]].
- [6] J. Beltran Jimenez and A. L. Maroto, JCAP **0903** (2009) 016 [[arXiv:0811.0566](#) [astro-ph]].
- [7] J. Beltran Jimenez, R. Lazkoz and A. L. Maroto, Phys. Rev. D **80** (2009) 023004 [[arXiv:0904.0433](#) [astro-ph.CO]].
- [8] J. Zuntz, T. G. Zlosnik, F. Bourliot, P. G. Ferreira and G. D. Starkman, Phys. Rev. D **81** (2010) 104015 [[arXiv:1002.0849](#) [astro-ph.CO]].
- [9] R. Cooke and D. Lynden-Bell, MNRAS **401**, 1409 (2010) [[arXiv:0909.3861](#) [astro-ph.CO]].
- [10] M. Thorsrud, D.F. Mota, S. Hervik, JHEP **1210**, 066 (2012) [[arXiv:1205.6261](#)].
- [11] R. A. Battye and A. Moss, Phys. Rev. D **74**, 041301 (2006) [[arXiv:astro-ph/0602377](#)].
- [12] R. A. Battye and A. Moss, Phys. Rev. D **76**, 023005 (2007) [[arXiv:astro-ph/0703744](#)].
- [13] R. A. Battye, M. Bucher and D. Spergel, [arXiv:astro-ph/9908047](#).
- [14] D.C. Rodrigues, Phys. Rev. D **77**, 023534 (2008) [[arXiv:0708.1168](#)].
- [15] S. Appleby, R. Battye and A. Moss, Phys. Rev. D **81**, 081301 (2010) [[arXiv:0912.0397](#) [astro-ph.CO]].
- [16] LSST Science Collaboration, [arXiv:0912.0201](#)
- [17] J. Sullivan et al, ApJ **737**, 102 (2011) [[arXiv:1104.1444](#)]
- [18] S. W. Hawking, Mon. Not. Roy. Astron. Soc. **142**, 129 (1969).
- [19] C. B. Collins and S. W. Hawking, Astrophys. J. **180**, 317 (1973).
- [20] J. D. Barrow, R. Juszkiewicz and D. H. Sonoda, Mon. Not. Roy. Astron. Soc. **213**, 917 (1985).
- [21] J. Barrow, Phys. Rev. D **55**, 7451 (1997) [[arXiv:gr-qc/9701038](#)].
- [22] J.D. Barrow and S. Hervik, Phys. Rev. D **81**, 023513 (2010) [[arXiv:0911.3805](#)].
- [23] M. Blomqvist, E. Mortsell, S. Nobili, JCAP **0806**, 027 (2008) [[arXiv:0806.0496](#)].
- [24] M. Blomqvist, J. Enander, E. Mortsell, JCAP **1010**, 018 (2010) [[arXiv:1006.4638](#)].
- [25] C. C. Dyer and R. C. Roeder, Astrophys. J. **180** (1973) L31.
- [26] R.M. Wald, Phys. Rev. D **28**, 2118 (1983).
- [27] H. K. Eriksen, F. K. Hansen, A. J. Banday, K. M. Gorski and P. B. Lilje, Astrophys. J. **605**, 14 (2004) [Erratum-  
ibid. **609**, 1198 (2004)] [[arXiv:astro-ph/0307507](#)].
- [28] K. Land and J. Magueijo, Phys. Rev. Lett. **95** (2005) 071301 [[arXiv:astro-ph/0502237](#)].
- [29] T. R. Jaffe, A. J. Banday, H. K. Eriksen, K. M. Gorski and F. K. Hansen, Astrophys. J. **629**, L1 (2005) [[arXiv:astro-ph/0503213](#)].
- [30] J. Hoftuft, H. K. Eriksen, A. J. Banday, K. M. Gorski, F. K. Hansen and P. B. Lilje, Astrophys. J. **699**, 985 (2009) [[arXiv:0903.1229](#) [astro-ph.CO]].
- [31] L. Campanelli, P. Cea and L. Tedesco, Phys. Rev. Lett. **97**, 131302 (2006) [Erratum-ibid. **97**, 209903 (2006)] [[arXiv:astro-ph/0606266](#)].
- [32] L. Campanelli, P. Cea and L. Tedesco, Phys. Rev. D **76**, 063007 (2007) [[arXiv:0706.3802](#) [astro-ph]].
- [33] R. Battye and A. Moss, Phys. Rev. D **80**, 023531 (2009) [[arXiv:0905.3403](#) [astro-ph.CO]].
- [34] T. Koivisto and D. F. Mota, JCAP **0808** (2008) 021 [[arXiv:0805.4229](#) [astro-ph]].
- [35] <http://www.darkenergysurvey.org>
- [36] <http://www.lsst.org/lsst>
- [37] L. Campanelli, P. Cea, G.L. Fogli, A. Marrone, Phys. Rev. D **83**, 103503 (2011) [[arXiv:1012.5596](#)].
- [38] E.F. Schlafly and D.P. Finkbeiner, ApJ **737**, 103 (2011) [[arXiv:1012.4804](#)].
- [39] A.J. Ross et al., MNRAS **424**, 564 (2012) [[arXiv:1203.6499](#)].
- [40] L. Anderson et al., MNRAS **427**, 3435 (2012) [[arXiv:1203.6594](#)].
- [41] H.V. Peiris and T.L. Smith, Phys. Rev. D **81**, 123517 (2010) [[arXiv:1002.0836](#)].
- [42] I.T. Iliev, G. Mellema, U-L. Pen, J.R. Bond, P.R. Shapiro, MNRAS **384**, 863 (2008) [[arXiv:astro-ph/0702099](#)].
- [43] X. Wang and W. Hu, ApJ **643**, 585 (2006) [[arXiv:astro-ph/0511141](#)].
- [44] L. Knox, R. Scoccimarro, S. Dodelson, Phys. Rev. Lett. **81**, 2004 (1998) [[arXiv:astro-ph/9805012](#)].
- [45] O. Zahn, M. Zaldarriaga, L. Hernquist, M. McQuinn, ApJ **630**, 657 (2005) [[arXiv:astro-ph/0503166](#)].
- [46] J.R. Pritchard, S.R. Furlanetto, M. Kamionkowski, MNRAS **374**, 159 (2007) [[arXiv:astro-ph/0604358](#)].
- [47] Planck Collaboration, [arXiv:astro-ph/0604069](#)
- [48] N. Afshordi, D.J.H. Chung, M. Doran, G. Geshnizjani, Phys. Rev. D **75**, 123509 (2007) [[arXiv:astro-ph/0702002](#)].